Conductance of atomic-scale Pb contacts in an electrochemical environment

F.-Q. Xie,[1] F. Hüser,[2] F. Pauly,[2] Ch. Obermair,[1] G. Schön,[2,3] and Th. Schimmel[1,3]
[1]*Institut für Angewandte Physik and DFG Center for Functional Nanostructures, Karlsruhe Institute of Technology, 76131 Karlsruhe, Germany*
[2]*Institut für Theoretische Festkörperphysik and DFG Center for Functional Nanostructures, Karlsruhe Institute of Technology, 76131 Karlsruhe, Germany*
[3]*Institut für Nanotechnologie, Karlsruhe Institute of Technology, 76344 Eggenstein-Leopoldshafen, Germany*
(Received 16 April 2010; revised manuscript received 4 July 2010; published 18 August 2010)

Atomic-sized lead (Pb) contacts are deposited and dissolved in an electrochemical environment, and their transport properties are measured. Due to the electrochemical fabrication process, deformation-induced mechanical strain is largely avoided, and we obtain conductance histograms with sharply resolved, individual peaks. Charge transport calculations based on density-functional theory for various ideal Pb contact geometries are in good agreement with the experimental results. Depending on the atomic configuration, single-atom-wide contacts of one and the same metal yield very different conductance values.

DOI: 10.1103/PhysRevB.82.075417 PACS number(s): 73.63.Rt, 82.45.Yz, 73.23.Ad, 31.15.es

Charge transport through nanostructures presently constitutes a highly active area of research, also due to its relevance for the further miniaturization of electronic devices.[1] Regarding atomic-sized metallic contacts, different experimental techniques have been developed for their fabrication, e.g., mechanically controllable break junctions (MCBJs),[2] modified scanning tunneling microscopes (STMs),[3] electromigration,[4] and electrochemical methods.[5,6] In MCBJ experiments and STM-based setups, under typical electrode separation speeds of more than 10 nm/s, atomic-sized contacts are formed by plastic deformation of the contact area.[1,7,8] In contrast, the advantage of the electrochemical deposition method is the absence of such deformation-induced mechanical strain during contact formation, resulting in corresponding differences in conductance histograms. This needs to be compromised, however, with the possible influence of the electrochemical environment on the conductance via molecular adsorption[5,9] and the surface tension at the solid-liquid interface.[10]

Conductance histograms of *s*-valent metals, such as gold, silver, or copper, have been analyzed extensively,[1,11,12] showing a preference for multiples of $G_0=2e^2/h$, with the peak at $1G_0$ being a very robust feature. As it is known that the chemical valence plays an important role for electron transport,[13,14] conductance histograms for multivalent metals may consequently show a very different shape.[1,12]

In this work, Pb will serve as a model system for multivalent metals. For Pb a broad peak between $1G_0$ and $3G_0$ was observed in conductance histograms based on the MCBJ technique.[15,16] During stretching of the junctions, the plateau regions of the conductance traces commonly exhibit a negative slope as a result of the mechanical strain.[13,17] With electrochemical techniques we have recently fabricated atomic-scale silver contacts with a high thermal and mechanical stability,[18] and exploited this for constructing gate-controlled atomic switches.[19,20] In this work, we study charge transport through atomic-sized Pb contacts in experiment and theory. The conductance histogram is compared to the literature and theoretical results for ideal contact geometries. In the density-functional theory (DFT)-based calculations we explore both "single-atom" and "dimer" geometries with a single atom or a chain of two atoms in the narrowest part of the junction, respectively. For these configurations we consider orientations of the semi-infinite electrodes along the three main crystallographic directions, namely, ⟨100⟩, ⟨110⟩, and ⟨111⟩.

Our experimental setup is illustrated schematically in Fig. 1. Since lead oxidizes under ambient conditions, the electrochemical cell is shielded in an inert gas chamber. Before starting with the electrochemical deposition, the chamber is thoroughly streamed with Ar. In this way, a practically oxygen-free environment is created for the growth of the atomic-sized Pb contacts. For their fabrication, two working electrodes (WEs) made of polycrystalline gold and separated by a gap of approximately 50 nm are prepared. They are covered with an insulating polymer coating except for the immediate contact area to minimize ionic conduction. Two lead wires (0.5 mm diameter, 99.998% purity) are used for the quasi-reference electrode (RE) and the counter electrode (CE). The potentials of the WEs with respect to the RE and the CE are set by a computer-controlled potentiostat. The electrolyte consists of 1 mM $Pb(NO_3)_2$+0.1M HNO_3 in bidistilled water. For conductance measurements an additional voltage of −12.9 mV is applied between the two WEs. To

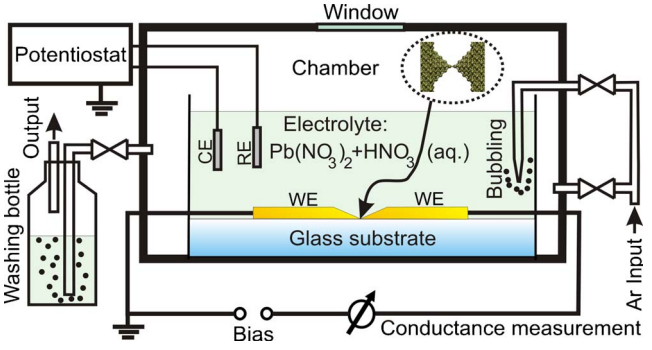

FIG. 1. (Color online) Schematic of the experimental setup. Pb is deposited and dissolved electrochemically in the narrow gap between two gold WEs on a glass substrate and the conductance of the contact is measured simultaneously. The potentials of the WEs with respect to the lead RE and the lead CE are set by a potentiostat.

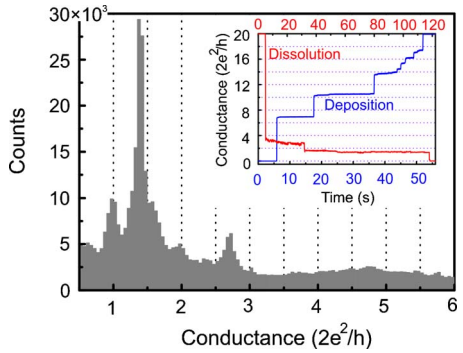

FIG. 2. (Color online) Conductance histogram of electrochemically fabricated atomic-sized Pb contacts. The inset shows two typical conductance-time traces for deposition and dissolution processes.

exclude possible specific effects of the gold WEs, contacts were also grown using Pb electrodes, yielding comparable results.

To fabricate the lead contact within the gap between the two WEs, a potential of 10–20 mV is applied to the RE. While lead is deposited in the junction, we monitor the conductance between the WEs. After contact deposition, the contact is dissolved again by setting the electrochemical potential of the RE to a value between −18 and −36 mV, and closed again by choosing the potential between 6 and 15 mV. By continuously repeating this procedure, conductance-time traces are recorded for a large number of opening and closing processes at a sampling rate of 50 ms.

Two typical conductance-time traces obtained for contact closing (deposition) and opening (dissolution) are shown in the inset of Fig. 2. The plateau regions in the traces are quite flat in general. This fact can be explained by the lack of mechanical strain during the electrochemical growth process, in contrast to contacts fabricated with the MCBJ or STM techniques, where mechanical deformations are involved.[6,13,14,17] The dissolution curve exhibits two plateaus at around $2.8G_0$ and $1.4G_0$. These values are consistent with the range of the rather continuously decreasing last conductance plateau, as reported in Refs. 13 and 17.

The main panel of Fig. 2 shows the conductance histogram, plotted with a bin size of $0.05G_0$. It represents the data from 1.5×10^6 conductance terraces in the range between 0 and $20G_0$ for both deposition and dissolution from 68 different samples, each terrace being stable longer than 200 ms. A dominant peak is found at $1.4G_0$ and additional ones at $1G_0$, $2G_0$, and $2.8G_0$. In the range from $3G_0$ to $6G_0$, the distribution is quite flat and shows a low broad maximum centered at around $4.8G_0$. The flat conductance-time traces and the features of the histogram with its peaks at $1.4G_0$ and $2.8G_0$ are compatible with observations in a similar electrochemical experiment.[6] We note, however, that only around 40 conductance-time traces were compiled in the conductance histogram of Ref. 6 so that the statistics appear too limited to allow for a more detailed comparison. On the other hand, the structure of our histogram differs markedly from that obtained with the MCBJ approach, where only a single, broad peak was observed between $1G_0$ and $3G_0$ and no detailed structure within this peak could be resolved.[15,16] The peak position at $1.4G_0$, however, is consistent with the results reported in Refs. 15 and 16. Since peaks in conductance histograms are caused by frequently occurring contact configurations, we naturally attribute the differences to the different set of atomic structures realized under the electrochemical fabrication conditions. While the electrolyte may have an influence via adsorbates and surface tension at the solid-liquid interface, they are distinguished particularly by the lack of accumulated mechanical strain and structural defects within the junction area. This interpretation is also consistent with the rather flat conductance-time traces observed here (Fig. 2, inset), as compared to those with slopes obtained with the MCBJ or STM approach.[13,17]

We note that the data from the 68 different samples, compiled in Fig. 2, yields similar individual conductance histograms. Since the gold WEs are polycrystalline, we can assume that the Pb electrodes meet in rather "random" configurations in the deposition-dissolution process for each device. This rules out the *simple* replication of specific contact configurations due to remnant Pb atoms at the WEs as the source of the sharp peaks in our conductance histograms, which might instead be possible for an individual sample.

In order to understand better the experimental findings, we have performed a theoretical analysis of charge transport through various Pb contacts. We describe their electronic structure at the level of DFT and determine the conduction properties within the Landauer approach using Green's-function techniques. Employing the RI-DFT module of TURBOMOLE 5.9,[21] we use BP86 as exchange-correlation functional[22,23] and the standard basis set "def-SVP" of split-valence quality augmented with *d*-like polarization functions.[24] An effective core potential efficiently deals with the innermost 78 electrons.[25] Our approach is described in detail in Ref. 26. Let us note that we determine parameters for the description of the electrodes from a spherical fcc cluster composed of 429 Pb atoms. The lattice constant for this cluster is set to the experimental value of 0.495 nm. The calculation yields $E_F=-3.76$ eV for the Fermi energy, a value roughly corresponding to the experimental work function of 4.25 eV.[27]

We investigate two types of junction configurations, namely, single-atom and dimer contacts (Figs. 3 and 4). For these we study different crystallographic orientations of the electrodes, namely, ⟨100⟩, ⟨110⟩, and ⟨111⟩. The electrodes are oriented along the z axis, the direction of charge flow. Such geometries are believed to be responsible for the first peak in conductance histograms of metals under ultrahigh-vacuum conditions. We consider only ideal geometries, where all atoms are located in the positions of the fcc lattice. The extended central clusters of Ref. 26, used for the description of the contacts, are composed of around 300 atoms. To keep the numerical effort manageable, their point-group symmetry is exploited.

Results for the single-atom contacts are displayed in Fig. 3. From the transmission at the Fermi energy, we obtain conductances of $2.7G_0$, $5.3G_0$, and $2.8G_0$ for the ⟨100⟩, ⟨110⟩, and ⟨111⟩ directions, respectively. At first glance, the conductance for the ⟨110⟩ direction is surprisingly high. However, as is visible in Fig. 3(d), this contact should better be

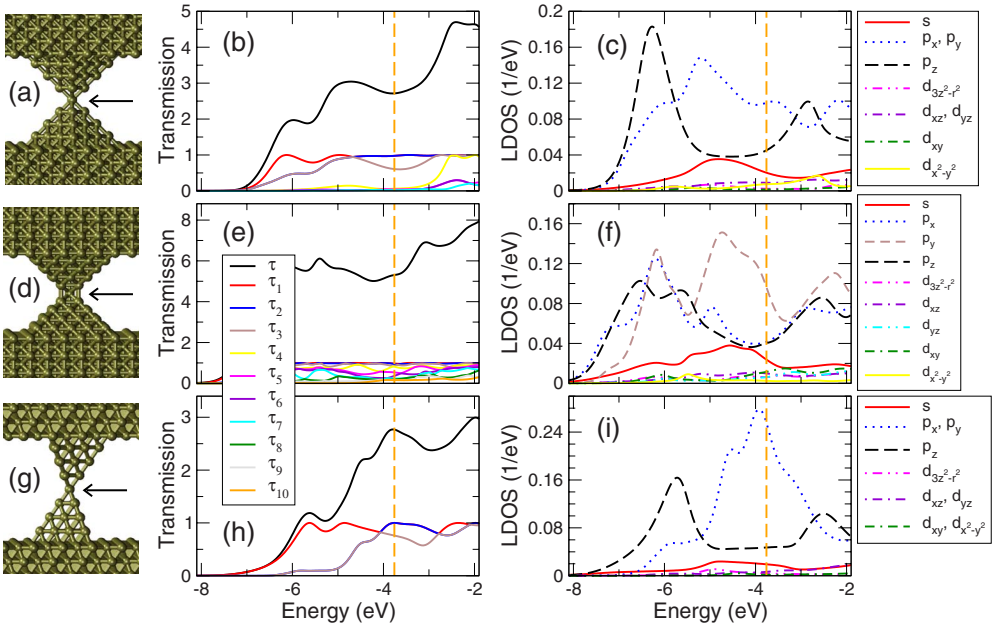

FIG. 3. (Color online) Geometries of single-atom contacts, their transmission as a function of the energy, and the LDOS of that atom in the narrowest part of the junction, which is indicated by an arrow in the geometries. The transmission $\tau=\Sigma_i\tau_i$ is resolved into the contributions τ_i from individual transmission channels and the LDOS into its orbital components (Ref. 26). The crystallographic orientation of the semi-infinite electrodes is [(a)–(c)] ⟨100⟩, [(d)–(f)] ⟨110⟩, and [(g)–(i)] ⟨111⟩, respectively. Vertical dashed lines indicate the Fermi energy at $E_F=-3.76$ eV.

considered as a "five-atom" contact due to the additional bonds resulting from the small distance between atomic layers. Therefore, we will henceforth refer to single-atom contacts as those for the ⟨100⟩ and ⟨111⟩ directions. For the latter two structures, the transmission at E_F is dominated by three transmission channels. In each case, the nondegenerate channel is of sp_z character while the two degenerate ones are p_x like and p_y like. The local density of states (LDOS) of the atom in the narrowest part of the constriction illustrates further the dominant role of the 6*s* and 6*p* states for conduction.

Due to the directional character of transport the point-group symmetries relevant for the classification of transmission channels in terms of irreducible representations are C_{4v}, C_{2v}, and C_{3v} for the structures with ⟨100⟩, ⟨110⟩, and ⟨111⟩ orientations, respectively, while their geometrical point groups are D_{4h}, D_{2h}, and D_{3d}. Degeneracies of channels, present for the ⟨100⟩ and ⟨111⟩ configurations, are therefore removed for ⟨110⟩. This fact will be more clearly visible for the dimer junctions with their lower conductance, but the same point-group symmetries, which we shall discuss next.

In Fig. 4 we illustrate the evolution of the conductance and of the total energy as a function of the distance *d* between the tip atoms for all the dimer contacts. All other distances are kept fixed in the stretching process. At the point of minimum total energy, conductances are $2.3G_0$, $1.6G_0$, and $2.8G_0$ for the ⟨100⟩, ⟨110⟩, and ⟨111⟩ contacts, respectively. As naively expected, the conductance exhibits a monotonous decay with *d* for ⟨100⟩ and ⟨110⟩. For ⟨111⟩, however, it stays rather constant. From an analysis of the LDOS of one of the chain atoms, we find that this is due to the p_x and p_y states, which move into resonance. As mentioned before, degeneracies of conduction channels are lifted for the ⟨110⟩ orientation as compared to the other junction configurations.

The peaks at $1.4G_0$ and $2.8G_0$ in our histogram of Fig. 2 are consistent with our theoretical results for single-atom and dimer structures, i.e., the first one can be ascribed to the ⟨110⟩ dimer while for the second one there are several possibilities such as a dimer along ⟨111⟩ or a single-atom contact along ⟨100⟩ or ⟨111⟩. This indicates that the contacts observed in the experiment resemble ideal lead junctions without strong contaminations or structural defects since they would lead to deviations from these conductance values. From our theoretical results, one may conclude that the peak at $2.8G_0$ should be higher than those at $1.4G_0$. The discussion of peak heights in the conductance histogram would, however, require the simulation of the electrochemical deposition and dissolution process in order to determine probabilities of occurrence for the contact structures. This would be a very time-consuming task with the DFT methods employed here.

The experimentally observed, pronounced peak at $1G_0$ is not predicted by the conductance calculations described above. However, as the contacts are in an aqueous electrochemical environment, small molecular species working as bridges between the two atomic-scale Pb electrodes, such as traces of H_2, O, O_2, or H_2O, might play a role.[9,16,28] Alternatively, ionic lead species could be taken into account, where specific transport channels of the junction are selectively suppressed. The interpretation of the peak at $1G_0$ as a result of the conductance quantization of a free-electron gas in a geometrical constriction, as observed in semiconductor heterostructures[29,30] and *s*-type metals,[1] appears as an oversimplification for multivalent metals.[16,31]

An alternative explanation of the peaks at $2G_0$ and $2.8G_0$ would be their interpretation as replicas of those at $1G_0$ and $1.4G_0$ with twice the value. Although geometries with paral-

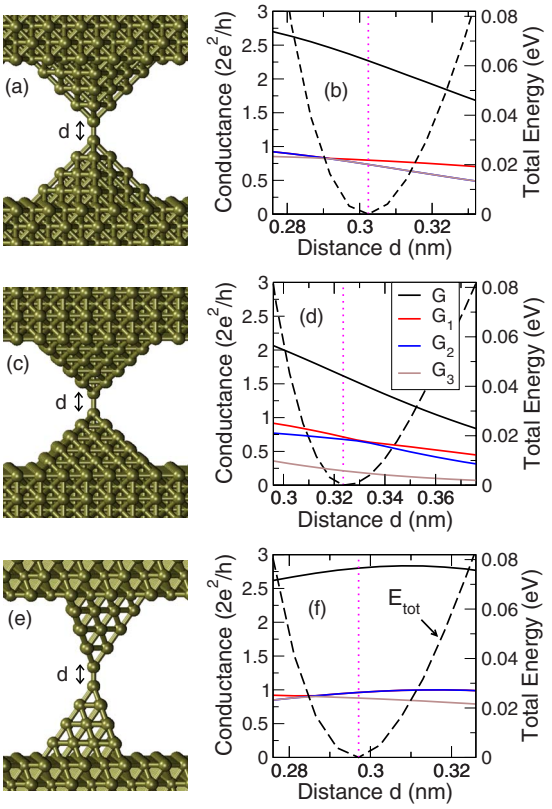

FIG. 4. (Color online) Dependence of the conductance G and the total energy E_{tot} on the distance d between the tip atoms for the different dimer configurations with [(a) and (b)] ⟨100⟩, [(c) and (d)] ⟨110⟩, and [(e) and (f)] ⟨111⟩ crystallographic orientation. In addition to $G=\Sigma_i G_i$ the contributions from the individual transmission channels $G_i=G_0\tau_i$ are shown. In each plot the y axis on the left refers to G and G_i (solid lines) and that on the right to E_{tot} (dashed lines). Dotted vertical lines indicate the distances d with minimal E_{tot}.

lel atomic wires were observed for STM-fabricated gold contacts,[32] no indications for the formation of similar structures exist for lead so far.

We note that the computed conductances are all within the range of the broad peak of MCBJ and STM measurements.[15,16] Furthermore, our analysis of transport using DFT is in agreement with theoretical results reported in Ref. 17. Employing a simpler tight-binding parametrization for describing the electronic structure and considering only the single-atom contact oriented along the ⟨111⟩ direction, the authors report the same conductance of $2.8G_0$. Keeping the central atom fixed, they find that the conductance stays practically constant when the junction is stretched, similar to our observations for the ⟨111⟩ dimer structure. They argue that the negative slopes of the conductance plateaus before contact rupture would require the inclusion of spin-orbit interactions. While such relativistic effects are considered in our calculations only in an effective manner through the core potentials,[25] our results show (see Fig. 4) that the dependence of the conductance on distance is strongly geometry dependent.

To summarize, the high thermal and mechanical stability and low strain in our electrochemically fabricated atomic-sized lead contacts makes it possible to resolve sharp conductance peaks and detailed substructures within the broad first peak in the conductance histograms obtained with MCBJ or STM techniques.[15,16] The theoretical analysis of transport within our DFT approach yields junction geometries compatible with the peaks at $1.4G_0$ and $2.8G_0$ and allows to attribute them to neutral single-atom and dimer contacts of Pb. The results demonstrate that the conductance of Pb contacts with a single-atom-wide constriction depends crucially on the contact geometry.

As an extension of this work, it might be interesting to explore, whether the MCBJ and STM approaches yield similar results to those reported here in the thermoactivated "self-breaking regime" at extremely low stretching rates under rather stress-free conditions.[8] Furthermore, the theoretical simulation of the growth process in the electrochemical environment to determine probabilities of occurrence for the contact structures would allow for a discussion of peak heights in the conductance histogram.

F.-Q.X. (experiment) and F.H. (theory) contributed equally to this work. We are grateful to M. Bürkle, A. Erbe, A. Halbritter, E. Scheer, and J. K. Viljas for fruitful discussions. This work was funded by the DFG and by the Baden-Württemberg Stiftung within the Network of Excellence "Functional Nanostructures." F.P. acknowledges support through a Young Investigator Group.

[1] N. Agraït, A. L. Yeyati, and J. M. van Ruitenbeek, Phys. Rep. **377**, 81 (2003).
[2] C. J. Muller, J. M. van Ruitenbeek, and L. J. de Jongh, Physica C **191**, 485 (1992).
[3] J. K. Gimzewski and R. Möller, Phys. Rev. B **36**, 1284 (1987).
[4] H. Park, A. K. L. Lim, A. P. Alivisatos, J. Park, and P. L. McEuen, Appl. Phys. Lett. **75**, 301 (1999).
[5] C. Z. Li, A. Bogozi, W. Huang, and N. J. Tao, Nanotechnology **10**, 221 (1999).
[6] J. Li, T. Kanzaki, K. Murakoshi, and Y. Nakato, Appl. Phys. Lett. **81**, 123 (2002).
[7] G. Rubio, N. Agraït, and S. Vieira, Phys. Rev. Lett. **76**, 2302 (1996).
[8] M. Tsutsui, K. Shoji, M. Taniguchi, and T. Kawai, Nano Lett. **8**, 345 (2008).
[9] O. Tal, M. Krieger, B. Leerink, and J. M. van Ruitenbeek, Phys. Rev. Lett. **100**, 196804 (2008).
[10] H.-J. Jin, X.-L. Wang, S. Parida, K. Wang, M. Seo, and J. Weissmüller, Nano Lett. **10**, 187 (2010).
[11] K. Hansen, E. Lægsgaard, I. Stensgaard, and F. Besenbacher, Phys. Rev. B **56**, 2208 (1997).
[12] B. Ludoph and J. M. van Ruitenbeek, Phys. Rev. B **61**, 2273

(2000).
[13] E. Scheer, N. Agraït, J. C. Cuevas, A. L. Yeyati, B. Ludoph, A. Martin-Rodero, G. R. Bollinger, J. M. van Ruitenbeek, and C. Urbina, Nature (London) **394**, 154 (1998).
[14] F. Pauly, M. Dreher, J. K. Viljas, M. Häfner, J. C. Cuevas, and P. Nielaba, Phys. Rev. B **74**, 235106 (2006).
[15] A. I. Yanson, Ph.D. thesis, Universiteit Leiden, 2001.
[16] P. Makk, S. Csonka, and A. Halbritter, Phys. Rev. B **78**, 045414 (2008).
[17] J. C. Cuevas, A. Levy Yeyati, A. Martín-Rodero, G. R. Bollinger, C. Untiedt, and N. Agraït, Phys. Rev. Lett. **81**, 2990 (1998).
[18] C. Obermair, R. Kniese, F.-Q. Xie, and T. Schimmel, in *Molecular Nanowires and Other Quantum Objects*, edited by A. S. Alexandrov, J. Demsar, and I. K. Yanson (Springer, New York, 2004).
[19] F.-Q. Xie, L. Nittler, C. Obermair, and T. Schimmel, Phys. Rev. Lett. **93**, 128303 (2004).
[20] F.-Q. Xie, R. Maul, C. Obermair, W. Wenzel, G. Schön, and T. Schimmel, Adv. Mater. **22**, 2033 (2010).
[21] R. Ahlrichs, M. Bär, M. Häser, H. Horn, and C. Kölmel, Chem. Phys. Lett. **162**, 165 (1989).
[22] A. D. Becke, Phys. Rev. A **38**, 3098 (1988).
[23] J. P. Perdew, Phys. Rev. B **33**, 8822 (1986).
[24] K. Eichkorn, F. Weigend, O. Treutler, and R. Ahlrichs, Theor. Chem. Acc. **97**, 119 (1997).
[25] W. Küchle, M. Dolg, H. Stoll, and H. Preuss, Mol. Phys. **74**, 1245 (1991).
[26] F. Pauly, J. K. Viljas, U. Huniar, M. Häfner, S. Wohlthat, M. Bürkle, J. C. Cuevas, and G. Schön, New J. Phys. **10**, 125019 (2008).
[27] P. A. Anderson and A. L. Hunt, Phys. Rev. **102**, 367 (1956).
[28] R. H. M. Smit, Y. Noat, C. Untiedt, N. D. Lang, M. C. van Hemert, and J. M. van Ruitenbeek, Nature (London) **419**, 906 (2002).
[29] B. J. van Wees, H. van Houten, C. W. J. Beenakker, J. G. Williamson, L. P. Kouwenhoven, D. van der Marel, and C. T. Foxon, Phys. Rev. Lett. **60**, 848 (1988).
[30] D. A. Wharam, T. J. Thornton, R. Newbury, M. Pepper, H. Ahmed, J. E. F. Frost, D. G. Hasko, D. C. Peacock, D. A. Ritchie, and G. A. C. Jones, J. Phys. C **21**, L209 (1988).
[31] A. I. Yanson and J. M. van Ruitenbeek, Phys. Rev. Lett. **79**, 2157 (1997).
[32] H. Ohnishi, Y. Kondo, and K. Takayanagi, Nature (London) **395**, 780 (1998).